Challenging metastatic breast cancer with the natural defensin PvD_1†

Tiago N. Figueira, ‡[a] Filipa D. Oliveira, ‡[a] Inês Almeida,[a] Érica O. Mello,[b] Valdirene M. Gomes,[b] Miguel A. R. B. Castanho *[a] and Diana Gaspar *[a]

Metastatic breast cancer is a very serious life threatening condition that poses many challenges for the pharmaceutical development of effective chemotherapeutics. As the therapeutics targeted to the localized masses in breast improve, metastatic lesions in the brain slowly increase in their incidence compromising successful treatment outcomes overall. The blood–brain-barrier (BBB) is one important obstacle for the management of breast cancer brain metastases. New therapeutic approaches are in demand for overcoming the BBB's breaching by breast tumor cells. In this work we demonstrate the potential dual role of a natural antimicrobial plant defensin, PvD_1: it interferes with the formation of solid tumors in the breast and concomitantly controls adhesion of breast cancer cells to human brain endothelial cells. We have used a combination of techniques that probe PvD_1's effect at the single cell level and reveal that this peptide can effectively damage breast tumor cells, leaving healthy breast and brain cells unaffected. Results suggest that PvD1 quickly internalizes in cancer cells but remains located in the membrane of normal cells with no significant damage to its structure and biomechanical properties. These interactions in turn modulate cell adhesiveness between tumor and BBB cells. PvD_1 is a potential template for the design of innovative pharmacological approaches for metastatic breast cancer treatment: the manipulation of the biomechanical properties of tumor cells that ultimately prevent their attachment to the BBB.

Introduction

Breast cancer is an invasive malignancy most commonly diagnosed in women and the second leading cause of cancer-related death in women worldwide.[1,2] Conventional cancer chemotherapy lacks specificity against tumor cells and displays low intracellular delivery efficacy. Additionally, severe side effects resulting from the unspecific cellular uptake by normal tissues and the development of resistance phenomena puts patients at a high risk of relapse.[3,4] Despite the many obstacles involved in the application of conventional chemotherapeutic strategies, these have been successful in increasing the lifespan of patients with breast cancer.[5] However, this increase in overall survival has been paired with

an increase in the incidence of metastatic cancer. As clinicians are in better control of the breast disease, lesions outside the breast have time to develop.[5–7] In fact, metastatic breast cancer accounts for most of the cancer deaths in breast cancer disease[8] and studies show that 10–16% of patients with disseminated breast cancer disease present lesions at the central nervous system (CNS), a percentage that can grow up to 30% after autopsy.[9,10] CNS relapse of patients with metastatic triple-negative breast cancer (TNBC) is particularly high.[11]

Challenges for breast cancer disease and respective brain metastatic lesions' management reside in the need for developing drugs that can recognize cancer cells and accumulate efficiently intracellularly. The treatment of brain metastasis by chemotherapy is, however, further compromised due to the inability of therapeutics to penetrate the blood–brain barrier (BBB) and accumulate in intracranial tissues.[5,12] In addition to the low passive paracellular permeability, the BBB cells express high levels of drug transporters that mediate drug efflux and consequently the brain is a protected location for malignant cells to settle and proliferate.[13,14] Other therapeutic options rely on whole brain radiotherapy and stereotactic radiotherapy, which have been correlated with cognitive impairment and surgical resection when multiple intracranial lesions are found, also with limited success.[15–17] Developing methods that can result in improved BBB penetration of drugs and their

[a]Instituto de Medicina Molecular, Faculdade de Medicina, Universidade de Lisboa, Av. Prof. Egas Moniz, Lisbon 1649-028, Portugal.
E-mail: dianagaspar@medicina.ulisboa.pt, macastanho@medicina.ulisboa.pt;
Fax: +351 217999477; Tel: +351 217985136
[b]Laboratório de Fisiologia e Bioquímica de Microrganismos do Centro de Biociências e Biotecnologia da Universidade Estadual do Norte Fluminense Darcy Ribeiro, Avenida Alberto Lamego 2000, Campos dos Goytacazes, Rio de Janeiro, 28013-602, Brazil
†Electronic supplementary information (ESI) available. See DOI: 10.1039/c7nr05872a
‡These authors contributed equally to this work.

availability in brain sites is of utmost importance and an urgent necessity. Peptide-based therapies have emerged as a pool of new strategies capable of overcoming unspecific targeting and resistance issues. Antimicrobial peptides (AMPs) with anticancer activity (anticancer peptides, ACPs) have been shown to exert effects directly on cancer cells[18] and of being capable of interfering with angiogenesis, gene expression and apoptosis, among other mechanisms.[19] Many natural AMPs have anticancer activities and have thus been explored as templates for drug design.[20–22] Our group has previously reported the apoptotic activity of the AMP human neutrophil peptide-1, HNP-1, on prostate cancer cells[23] highlighting ACPs' potential in blocking the metastatic cascade. In the present work, we reveal the antitumor activity of PvD_1 peptide, an AMP defensin from *Phaseolus vulgaris*, the common bean,[24,25] on human breast cancer cells and its ability in aiding the prevention of brain metastasis formation by affecting cellular adhesion. By using a combination of spectroscopic, fluorescence and imaging techniques we show that PvD_1 peptide acts directly on cancer cells from the primary tumor location and directly on the adhesion of breast cancer cells to the endothelial cells from the human BBB without significant impact on cells from normal tissue. By understanding the cellular and molecular interactions occurring in the initial moments of cell–cell contact, an alternative mechanism of action for anticancer treatment is envisioned based on the prevention of the metastatic cells' BBB crossing and reaching into the brain parenchyma. At the same time, a new avenue for the role of diet nutraceuticals in breast cancer therapy is open.

Experimental

Reagents

Human neutrophil peptide-1 (HNP-1; Ala-Cys-Tyr-Cys-Arg-Ile-Pro-Ala-Cys-Ile-Ala-Gly-Glu-Arg-Arg-Tyr-Gly-Thr-Cys-Ile-Tyr-Gln-Gly-Arg-Leu-Trp-Ala-Phe-Cys-Cys: Cys2-Cys30, Cys4-Cys19, Cys9-Cys29) was purchased from Bachem. Adherent cell lines MDA-MB-231 and MCF 10A were purchased from American Type Culture Collection (ATCC, HTB-26 and CRL-110317 respectively). HBMEC (human brain microvascular endothelial cells) isolated by ScienCell Research Laboratories from human brain tissue and respective media and supplements were purchased from Innoprot. DMEM media, heat-inactivated fetal bovine serum (FBS), penicillin and streptomycin solution, and trypsin (TrypLE Express enzyme) were obtained from Life Technologies. Mammary Epithelial Basal Medium (MEBM) and SingleQuots (hydrocortisone, bovine pituitary extract (BPE), epidermal growth factor human recombined (rhEGF), and recombinant human insulin) were purchased as clonetics MEGM™ BulletKit™ from Lonza, Ltd. Cholera toxin from *Vibrio cholera*, trypsin inhibitor from *Glycine max* (soybean), glutaraldehyde solution (50% in water), bovine-serum albumin biotinamidocaproyl labeled (biotin-BSA), streptavidin, concanavalin A (ConA, biotin conjugate) and dimethyl sulfoxide (DMSO) were obtained from Sigma-Aldrich. MTT (3-(4,5-di-methylthiazol-2-yl)-2,5-diphenyltetrazolium bromide) salt was obtained from Invitrogen™ (Carlsbad, CA, USA) and 4-(2-[6-(dioctylamino)-2-naphthalenyl]ethenyl]-1-(3-sulfopropyl)pyridinium inner salt (di-8-ANEPPS) probe was purchased from Sigma-Aldrich.

PvD_1 peptide

The purification of $PvD1$, the defensin from *Phaseolus vulgaris* (cv. Pérola) seeds, was performed as described by Games *et al.*[24] For the protein extraction, *P. vulgaris* seeds were pilled and the cotyledons were ground to a fine flour which was mixed with phosphate buffer (10 mM Na_2HPO_4; 15 mM NaH_2PO_4; 100 mM KCl; 1.5% EDTA) pH 5.4 at a 1:5 ratio (flour : extraction buffer) and stirred for 2 h at 4 °C. This homogenate was centrifuged (15 000g, 20 min at 4 °C) and the supernatant was subjected to ammonium sulfate precipitation at 70% saturation. After centrifugation, the precipitate was solubilized in distilled water and heated at 80 °C for 15 min. This protein extract was then centrifuged (10 000g, 8 min at 4 °C) and the obtained supernatant was dialyzed against distilled water and recovered by freeze drying for further purification of $PvD1$. Initially an anion-exchange DEAE-Sepharose column was employed. The sample was firstly eluted in the equilibration buffer Tris-HCl 20 mM, pH 8.0 and then in a Tris-HCl buffer added with 1 M NaCl. These chromatographic steps were performed at a flow rate of 60 mL h^{-1} (LKB pump P-1, Pharmacia). The absorbance of the fractions was read on a spectrophotometer at 280 nm. The D1 fraction, the non-retained fraction derived from the previous anion-exchange chromatography on a DEAE-Sepharose column, was solubilized in 0.1% TFA and 500 μL were injected into the C18 reverse phase column. Chromatography was performed at a flow rate of 0.5 mL min^{-1} with 100% solvent A (0.1% TFA and 2% acetonitrile) for 10 min, 0–100% solvent B (80% acetonitrile containing 0.1% TFA) over 30 min, 100% solvent B over 5 min and finally 100% solvent A for the remaining time. Proteins were monitored by on-line measurement of the absorbance at 220 nm. The peak corresponding to the $PvD1$ was collected.

Cell culture

MDA-MB-231 adherent human breast cancer cells were cultured as a monolayer in DMEM supplemented with 10% FBS and 1% penicillin–streptomycin. MCF 10A human breast cells were cultured as a monolayer in MEBM supplemented with the respective SingleQuots according to manufacturer's instructions, cholera toxin 100 ng ml^{-1} and 1% penicillin–streptomycin. Human Brain Microvascular Endothelial Cells (HBMEC) were cultured in fibronectin (FN)-coated flasks (2 μg cm^{-2}) in endothelial cell basal medium with 5% FBS, 1% penicillin–streptomycin and 1% endothelial cell growth supplement. All cultures were maintained at 37 °C and 5% CO_2 in a humidified environment.

Cellular proliferation assay

An MTT assay was used for evaluating the *in vitro* cytotoxic activity of HNP-1 and PvD_1 peptides as previously described.[26]

MDA-MB-231 and MCF 10A cells were seeded at 3000 cells per 100 μL per well and 50 000 cells per 100 μL per well, respectively, into a 96-well plate and incubated for 24 h. HBMEC were seeded at 5000 cells per 100 μL per well into 96-well plates coated with FN (2 μg cm^{-2}) and incubated also for 24 h. After media removal, 100 μL of the peptide solution prepared in complete serum-free medium and ranging from 0.01–100 μM for PvD$_1$ and 0.1–100 μM for HNP-1 was added to the wells. After a 24 h incubation period with the peptides, 10 μL of 5 mg ml^{-1} MTT solution was added to each well following a 2 h incubation. The medium containing peptide and MTT was then removed and 150 μL of DMSO (spectrophotometric grade) was added for solubilisation of the formed formazan crystals. Absorbance was measured at 540 nm. Serum-free medium, 20% DMSO-containing medium and 30% DMSO-containing medium were used as controls for 100% cell viability (untreated cells) and negative controls for breast tumor cells/HBMEC and breast normal cells, respectively.

Cell viability (%) was determined as: (Absorbance$_{peptide-treated \ cells}$/Absorbance$_{untreated \ cells}$) × 100 and cell death (%) as: 100 − (percent viability). IC$_{50}$ values were determined using the Graphpad 6.0 software package using a log(inhibitor) $vs.$ normalized response. Experiments were performed on different days using independently grown cell cultures.

Atomic force microscopy imaging

AFM imaging was performed with a JPK Nano Wizard II (Berlin, Germany) mounted on a Zeiss Axiovert 200 inverted microscope (Carl Zeiss, Germany). The AFM head is equipped with a 15 μm z-range linearized piezoelectric scanner and an infrared laser. Human breast tumor cells were cultured at 1 × 10^4 cells per ml while human breast non-tumor cells were seeded at 1 × 10^5 cells per ml into 40 mm tissue culture dishes (TPP) for 24 h. HBMEC were cultured at 1 × 10^4 cells per ml into 40 mm tissue culture dishes previously coated with FN (2 μg cm^{-2}). Cells were washed with phosphate buffered saline (PBS) solution and serum-free medium containing PvD$_1$ and HNP-1 was added. Control cells were prepared with serum-free medium only. After a 24 h incubation cell medium was removed and cells were washed with PBS solution and incubated with a 1% glutaraldehyde solution for 10 minutes (room temperature), washed with PBS and sterile milli-Q water and finally air-dried. Images were obtained in air using intermittent contact and contact mode. Uncoated silicon ACL cantilevers from AppNano with typical resonance frequencies ranging between 145–230 kHz and an average spring constant of 45 N m^{-1} were used. Scan speeds were lower than 1 Hz and total areas with 100 × 100 μm were scanned with a 512 × 512 pixel resolution. Height and error images were recorded and line fitted as required.

The presented cell height corresponds to the difference between the bottom and the highest point of each cell and the maximum cell height was acquired after drawing height profiles for each cell using JPK SPM Data Processing version 5.1.8. The total number of analyzed cells was 135, 151 and 59 for MDA-MB-231, MCF 10A and HBMEC respectively. The surface roughness for control and treated cells was defined as the root-mean-square roughness (R_{ms}) obtained from AFM height images. Gwyddion software version 2.33[27] was used for the determination. R_{ms} values were obtained from squared areas of 2.5 × 2.5 μm in the nucleus and cytoplasm areas. The R_{ms} average of groups of five squares corresponds to the R_{ms} value of each cellular component, nuclei and cytoplasm, within each cell. Final R_{ms} values correspond to averages obtained for a total number of 54, 51 and 50 cells for MDA-MB-231, MCF 10A and HBMEC respectively. Cells were observed and imaged through two to three different days using independently grown cultures.

Zeta potential measurements of live human breast and microvascular endothelial cells (HBMEC) in the presence of the PvD$_1$ peptide

Confluent human breast and endothelial brain cells were washed after trypsinization and diluted in PBS buffer to 1 × 10^5 cells per ml and 2.5 × 10^5 cells per ml, respectively. Cell suspensions with and without PvD$_1$ (0.01–50 μM) were added into disposable zeta cells with gold electrodes and allowed to equilibrate for 30 minutes at 37 °C. Each experiment consisted of 10–15 measurements with ∼40–70 runs performed at a constant voltage (40 V) using a Zetasizer Nano ZS. The complete experiment was carried out at least two times using independent cellular suspensions.

Di-8-ANEPPSs labelling of live human breast and microvascular endothelial cells and fluorescence spectroscopy evaluation in the presence of PvD$_1$

Cells from human breast and brain were washed, suspended in PBS buffer and incubated with 30 μM of di-8-ANEPPS. The cells were allowed to incorporate the fluorescent probe for 1 h at room temperature at constant rotation, and were then washed to remove non-incorporated di-8-ANEPPS and suspended to a final concentration of 5 × 10^5 cells per ml. Cell membrane dipole potential variations in the presence of PvD$_1$ were examined through di-8-ANEPPS fluorescence excitation spectrum shifts.

Di-8-ANEPPS fluorescence excitation spectra were collected on an Edinburgh FLS920 spectrofluorimeter (Livingston, UK). The emission wavelength, λ_{emi}, was set to 670 nm to avoid membrane fluidity artifacts,[28] and individual spectra were retrieved between 380 and 580 nm in the absence and presence of PvD$_1$ (10 minute incubation). Excitation spectra were corrected for background intensity. Differential spectra were obtained by subtracting the normalized excitation spectra (to the spectrum integral) of the suspended labeled cells in the presence of PvD$_1$ from the control spectra, obtained in the absence of the peptide.[29] To quantify di-8-ANEPPS spectral shifts, excitation intensity ratios (R) were calculated through the relationship $R = [I_{exc}(\lambda_a)]/[I_{exc}(\lambda_b)]$, where λ_a and λ_b correspond to the wavelengths with the highest absolute intensity difference (differential spectrum minimum or maximum). For a correct interpretation, λ_a and λ_b should be lower and higher than the maximum excitation wavelength, respectively. The intensity ratios normalized to the control R (R_{norm}) were used as a quantitative parameter of di-8-ANEPPS spectral shifts and

correlate with variations in the cell membrane dipole potential. This experiment was repeated on two different days using independently grown cell cultures.

Atomic force microscopy-single cell force spectroscopy (AFM-SCFS)

AFM setup. A NanoWizard II AFM from JPK Instruments (Berlin, Germany) mounted on the top of an Axiovert 200 inverted microscope (Carl Zeiss, Germany) was used which was coupled with a CellHesion module (JPK Instruments) for extending the vertical range of the AFM from 15 μm to 100 μm. Experiments were conducted at constant temperature, 25 °C, using a temperature-controlled BioCell sample chamber from JPK Instruments.

Cantilever coating. SCFS measurements were performed using tipless arrow TL1 cantilevers (Nanoworld, Neuchatel, Switzerland) with a nominal spring constant of 0.03 N m^{-1}. Cantilevers were cleaned for 15 minutes with UV light and then coated with biotin BSA-ConA-streptavidin as previously described.[30] Briefly, after a PBS rinse, cantilevers were incubated overnight with a biotin-BSA solution (0.5 mg ml^{-1}) at 37 °C under a humidified atmosphere, rinsed with PBS, incubated for 30 minutes at room temperature under a humidified atmosphere with streptavidin (0.5 mg ml^{-1}), rinsed again with PBS and incubated 30 minutes with a ConA-biotin solution (0.4 mg ml^{-1}) maintaining conditions. Cantilevers were coated for each day of measurement, kept in PBS buffer until use and calibrated using the inbuilt thermal noise method before each experiment.

Cell culture

Breast tumor cells and HBMEC were grown onto coverslips (FN coated at 2 μg cm^{-2} for HBMEC) at 1×10^4 cells per ml for 24 h. Control and PvD_1-treated cells were prepared as described for AFM experiment imaging but kept without fixation procedures for further use in SCFS experiments.

Cell capture

Isolated cell suspensions of breast tumor and brain endothelial cells were obtained from confluent cells cultured in separated flasks, before each experiment, without trypsinization and after 30 minutes of incubation in PBS. Detached cells were washed, suspended in serum-free medium and incubated for 15 minutes at 37 °C with agitation for recovering of the collection procedures. Cells grown over the coverslips were mounted on the BioCell chamber and kept within serum-free medium. Around 10^3 harvested cells were injected into the chamber and allowed to settle for a few seconds. Cell capture was performed by positioning a ConA-biotin-coated cantilever over a settled breast tumor or brain endothelial cell and establishing contact for 30 seconds. The cantilever with the captured cell was slowly retracted and the attached cell was allowed to rest and establish firm contact with the cantilever for 5 minutes away from the surface.

Cell–cell adhesion experiments. Cell–cell contact was promoted at constant height with a speed of 2 μm s^{-1}, in closed-loop mode and with an applied force of 0.5 nN. Contact time was 5 seconds and the cantilever was further retracted with a

z-range displacement of 70 μm to guarantee complete cell separation. One to five force–distance curves were obtained for each contact with a 10 second interval between each curve and 30 second interval between the cells probed. Detachment force (F_D), detachment work (W_D) and tether extraction forces were obtained from the retraction force curves using the Image Processing Software 5.1.8 (JPK Instruments, Berlin, Germany). Data sets were generated using between 16 and 28 cells. Cantilever cell-bound and coverslip cell-attached morphology was constantly assessed during experiments to guarantee viability.

Statistical analysis. Quantitative data were processed using Excel 2007 (Microsoft, USA) and the GraphPad Prism 6.0 software package. Medians, means and standard deviations are shown in the figures. Pairwise significances were calculated using one-way ANOVA followed by Tukey's multiple comparison test, and nonparametric Mann–Whitney, Kruskal–Wallis and two-tailed unpaired t-tests.
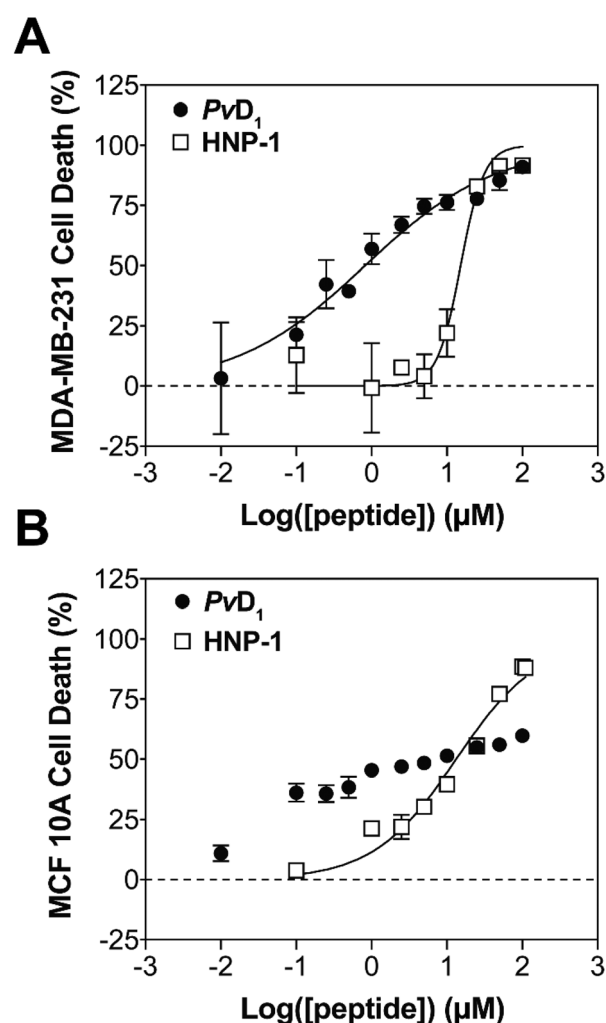

Fig. 1 *In vitro* cytotoxicity of PvD_1 and HNP-1 toward human breast cells. The cytotoxic activity of PvD_1 and HNP-1 was tested using MDA-MB-231 breast adenocarcinoma cells (A) and MCF 10A breast epithelial cells (B). All experiments were repeated on different days using independently grown cell cultures.
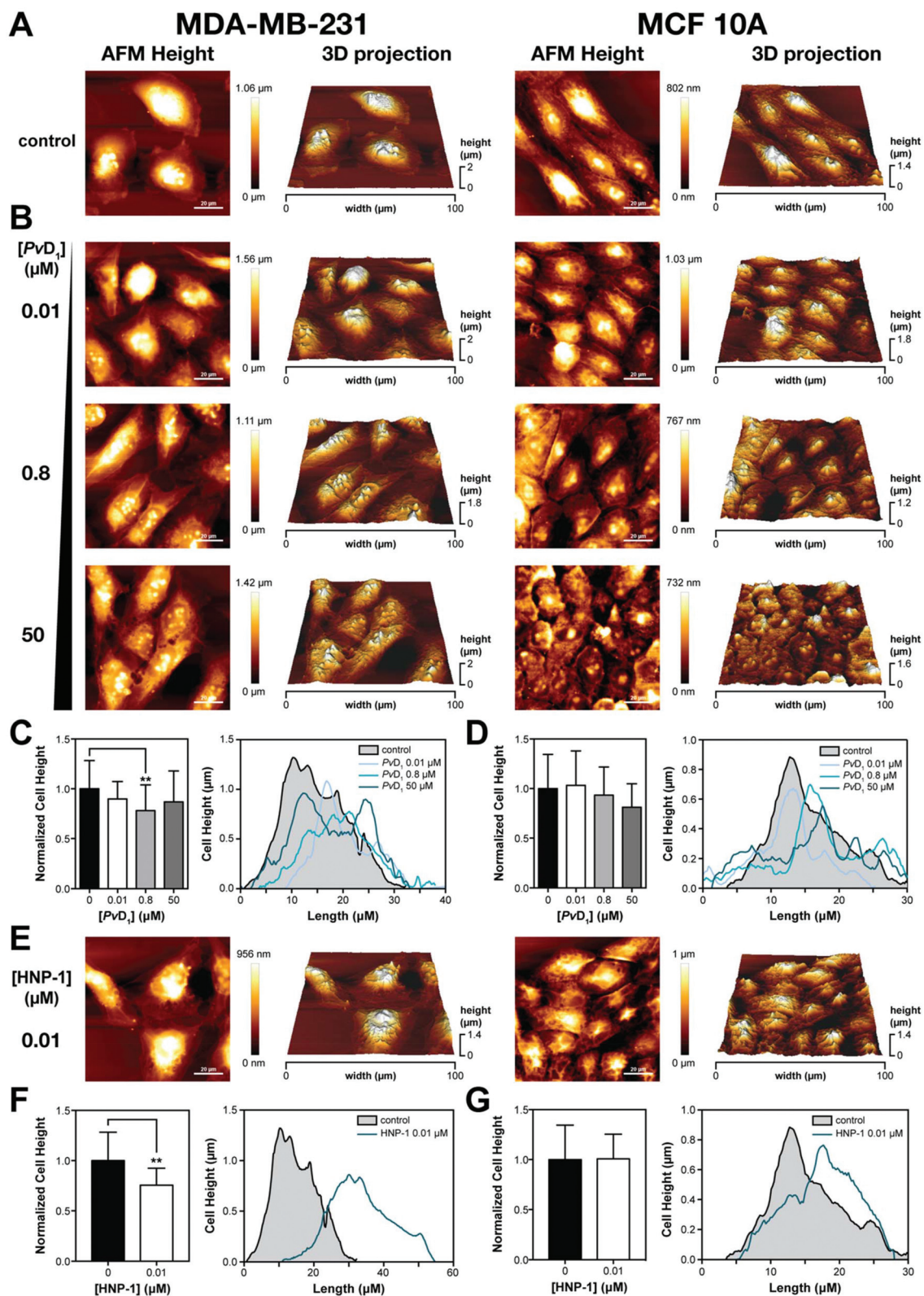
Fig. 2   Cell morphological examination of human breast cells using atomic force microscopy (AFM). Representative AFM height images of human breast cells in the absence (A) and the presence of PvD_1 (B) and HNP-1 (E). Control cells present epithelial morphology that change in the presence of both peptides. Representative cell height profiles and cell height normalized to control determined before and after PvD_1 and HNP-1 contact are shown (C, D, F, G). The number of analysed cells for the determination of MDA-MB-231 cell height in the presence of PvD_1 was: 0 μM − 45; 0.01 μM − 22; 0.8 μM − 33 and 50 μM − 23 while for the MFC 10A cell line: 0 μM − 28; 0.01 μM − 45; 0.8 μM − 41 and 50 μM − 25. Cell height determination in the presence of HNP-1 was based on 12 cells for both cell lines.

Results and discussion

Developing more effective and selective anticancer drugs remains one of the greatest and most urgent challenges in medicine. Whereas early and more effective diagnostics coupled with current therapies are increasingly successful, metastatic disease increases cancer incidence. TNBC, for instance, has high metastatic ability to the CNS. In fact, most of brain metastases seen in patients have their origin in malignant melanoma, lung and breast cancers.[31] These patients need a chemotherapeutic agent that reaches the brain parenchyma for targeting these metastatic lesions.

PvD_1 peptide is an efficient ACP against breast tumor cells and acts on an intracellular target

The *in vitro* activity of both PvD_1 and HNP-1 was studied using one breast cancer cell line: MDA-MB-231 (breast adenocarcinoma) and one normal human cell line: MCF 10A (breast epithelial cells). Cell lines were exposed to increasing concentrations of peptides for 24 h (Fig. 1). MTT assay resulted in IC$_{50}$ values of 0.82 ± 0.14 and 15.2 ± 1.6 μM for PvD_1 and HNP-1 respectively, against the cancer cell line. The selectivity of both peptides was further investigated using healthy breast cells revealing an IC$_{50}$ value of 13.3 ± 1.8 μM for HNP-1. The curve obtained for PvD_1-normal breast cell assay deviated significantly from the typical sigmoidal profile: cell death is only weakly dependent on concentration and 100% cell death was not reached within the range of concentrations tested. Overall, PvD_1 shows much higher efficacy towards breast cancer cells when compared with the standard reference defensin HNP-1 and other ACPs.[18,32]

AFM is a technique of excellence for observing changes in cells with nanometre resolution[33,34] and was used for a morphological and topographical examination of the reference standard defensin HNP-1 and PvD_1 peptides' effect on tumor and normal breast cells. Representative AFM height images and respective 3D projections are presented in Fig. 2. The results show a higher efficacy of PvD_1. Tumor and normal breast cells show an epithelial morphology and variable dimensions (Fig. 2A) with a similar topography as expected.[35] An intact surface is observed with pseudopodia and filopodia in the case of tumor cells (structures associated with high invasive potential) while normal cells show no evidence of these structures. Increasing PvD_1's concentration results in damage of the breast tumor cells characterized by nuclear collapse, cell shrinkage and visibility of the cytoskeleton structure (Fig. 2B) concomitant with changes in height (Fig. 2C). No alterations were observed however at the membrane roughness (R_{ms}) level (Fig. S1†). In normal breast cells PvD_1 effects appear to be attenuated with no observed changes in the cell height and cell membrane roughness (Fig. 2D and S1†). Considering that the cytoskeleton, in addition to acting as the cell backbone, is also responsible for maintaining the lipid bilayer integrity,[36] changes observed in the cell height and the maintenance of R_{ms} support the hypothesis that despite the peptide's aggressiveness towards tumor cells, cellular structure and integrity are partially retained. Consequently, PvD_1 activity must result from an intracellular target.

The effects of HNP-1 on breast cells are also depicted in Fig. 2E–G. At concentrations below the IC$_{50}$ visible morphological alterations occur in the tumor cells. Changes in the nuclear area reveal nuclear collapse supported by variation of
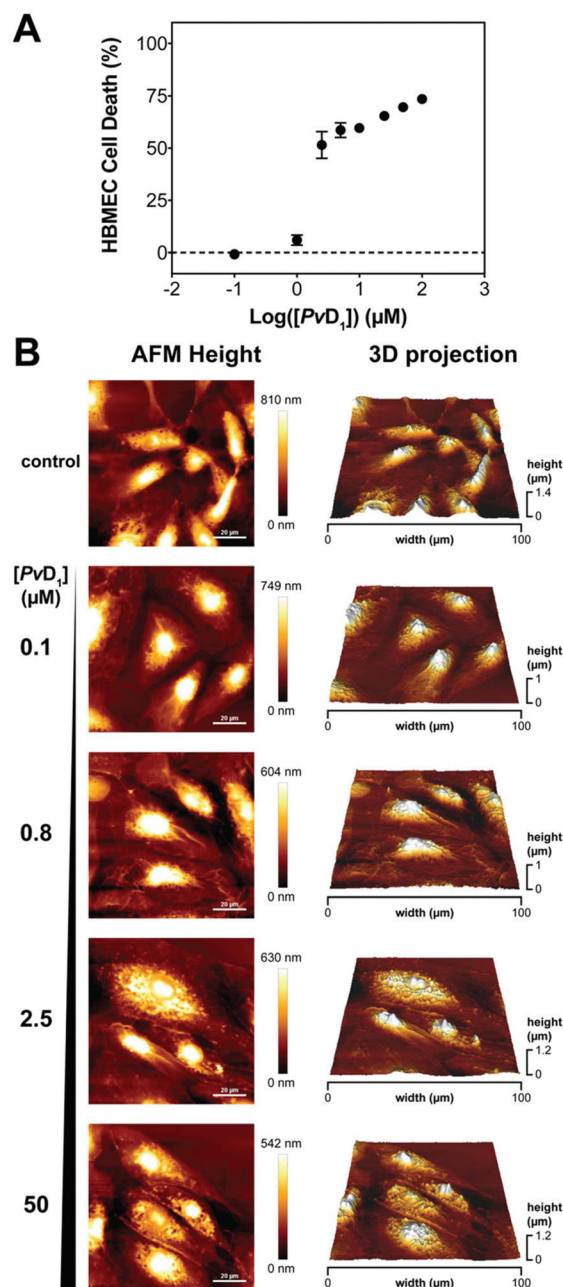

Fig. 3 *In vitro* cytotoxicity of PvD_1 toward human brain microvascular endothelial cells (HBMEC) and cellular characterization by atomic force microscopy (AFM). The cytotoxic activity of PvD_1 was additionally tested using HBMEC (A). PvD_1's effects on HBMEC were also investigated by AFM at the single cell level. Representative AFM height images of HBMEC in the absence and presence of PvD_1 are shown which reveal a selective activity for the peptide (B).

cell height profiles (Fig. 2F). Cytoskeleton changes are also evident as the cell backbone becomes visible. We could also observe small solid structures near the nuclear area of the cells, characteristic of apoptotic bodies.[37] No significant changes were observed at the cell membrane roughness level when compared with the untreated control cells (Fig. S1†). Normal breast cells treated with HNP-1 at low concentrations showed important morphological defects. Cells appeared shrunk with their cytoskeleton structure evident, however no changes in the cell height and membrane roughness were observed (Fig. 2G and S1†). Increasing concentrations of HNP-1 led to severe cellular damage that compromised a detailed examination of the different cellular parameters used for evaluating the peptide's activity.

PvD_1 interacts with human breast and brain cellular membranes resulting in reduced cytotoxic activity and cellular damage of the human brain cells

After studying PvD_1 effects at the breast tumor level, we further explored the effects of this peptide directly on human brain microvascular endothelial cells. The cell proliferation assay result is similar to the one obtained in MCF 10A cells (Fig. 3A), with 50% cell death at ∼7 μM.

AFM analyses of HBMEC in the presence of PvD_1 revealed the reduced impact that the peptide has over cell morphology and topography. In the absence of PvD_1 cells appear elongated

with a distinct nuclear area (Fig. 3B). The presence of the peptide allows the visualization of the cytoskeleton structure whereas nuclear condensation and fragmentation is also observed. PvD_1 concentrations near 50 μM, induce changes in cell shape and accentuate nuclear damage. These changes are however accompanied by no alterations in cell membrane roughness or the maximum cell height (Fig. S2†). Despite the observed low cell damage induced by $PvD1$, a peptide–membrane interaction cannot be excluded at this point and so PvD_1 interaction with tumor and normal cell membranes was assessed by zeta potential and fluorescence spectroscopy techniques in the absence and presence of increasing peptide concentrations (Fig. 4 and S3†).

Mean values obtained for the surface zeta potential of breast cancer cells, breast normal cells and brain endothelial cells were -22.99 ± 2.75; -25.0 ± 0.87 mV and -12.86 ± 0.74, respectively (Fig. 4B and C). The obtained HBMEC's membrane surface charge value is similar to the one reported by our group for bovine endothelial cells (BCEC)[38] and to the one we obtained for a primary culture of HBMECs (-13.73 ± 0.78 mV, data not shown) cultured as described by Bernas and co-workers.[39] The presence of zwitterionic phospholipids in normal cells contributes to an overall neutral charge[19,40] of the membrane but zeta potential reports on the electrostatic potential formed at the slipping plane of the cell[32] and consequently results from an overall charge for which not only the
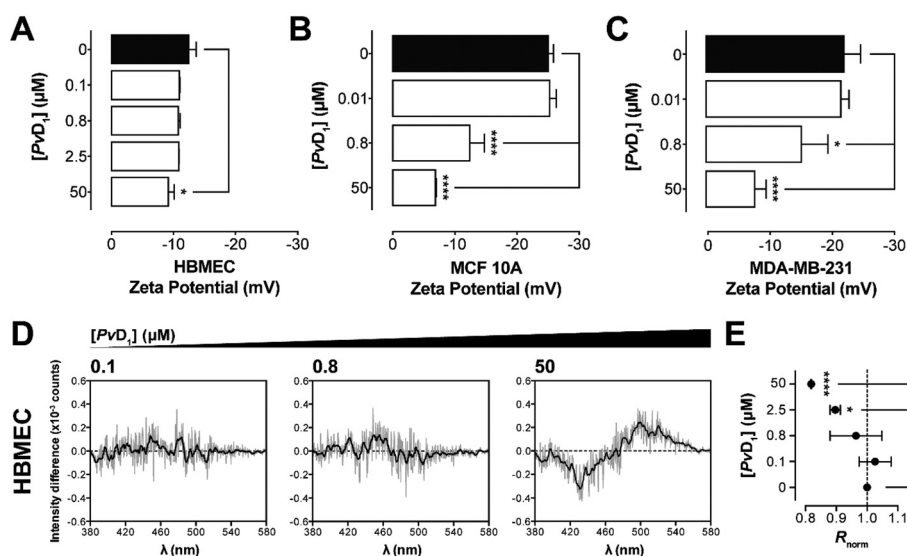

Fig. 4 Cell membrane surface charge of human breast and brain microvascular endothelial cells in the presence of PvD_1 and changes in the dipole potential of human brain cells' membranes. PvD_1 peptide effects on the cell membrane charge density of HBMEC (A), MCF 10A (B), and MDA-MB-231 (C) cells were followed by zeta potential measurements. All experiments were repeated on different days using independently grown cell cultures. A one-way ANOVA followed by a Tukey *post hoc* test was employed. *$0.01 < p$-value < 0.05; ****p-value < 0.0001. Variations in the cell membrane dipole potential of HBMEC in the presence of PvD_1 were also followed by di-8-ANEPPS fluorescence excitation spectra shifts (D, E). This voltage sensitive probe incorporates into the outer leaflet of the cellular membrane and is sensitive to changes in the local electric field derived from the alignment of water and lipid headgroup dipoles. Differential spectra were obtained by subtracting the normalized excitation spectra (to the integrated spectrum areas) of the suspended labeled cells in the presence of increasing PvD_1 concentration from the spectra obtained in the absence of PvD_1 (D). For clarity, a smoothed differential excitation spectrum is presented for each condition. The normalized excitation intensity ratios, R_{norm}, determined at different PvD_1 concentrations, are shown (E). This ratiometric analysis was used to quantify the extent of di-8-ANEPPS spectra deviation and, consequently, the magnitude of membrane dipole perturbation. All experiments were repeated on different days using independently grown cell cultures. Statistical significance was evaluated with an unpaired two-tailed t-test. *$0.01 < p$-value < 0.05; ****p-value < 0.0001.

lipid headgroups of the membrane bilayer contribute but also ions and charged proteins.[38] The anionic character of the BBB is a key feature for selective crossing of cationic molecules into the brain.[38] The loss of lipid asymmetry leads to the accumulation of phosphatidylserine (PS) phospholipid at the outer leaflet of the membrane bilayer of tumor cells and also the overexpression of O-glycosylated mucins, glycosaminoglycans (GAGs) and accumulation of sialic acid (SA) residues is expected.[19,41,42] MCF 10A epithelial cells are positive for sialomucins, cytokeratins and milk fat globe antigen and even though they may display a neutral net charge on the plasma membrane, the presence of sialomucins can strongly contribute to the high negative surface charge value measured.

Zeta potential variation results revealed a marked affinity of PvD_1 for breast cell membranes (Fig. 4B and C). PvD_1 interacts with both types of breast cells permeabilizing the membrane and not leading to complete surface charge neutralization. For HBMEC, changes in the surface charge density were only observed at high peptide concentrations (Fig. 4A), in which more than 60% of the cells were non-viable. High PvD_1 concentration is needed to significantly affect zeta potential values but cell death occurs without full neutralization of the membrane charge, such as we have previously described for other ACPs.[23,32]

Mechanistic insights into peptide–membrane interaction were further obtained after labelling live HBMEC and breast cells with the voltage-sensitive dye, di-8-ANEPPS. This fluorescent probe is incorporated into the outer leaflet of the cellular membranes and senses the local electric field derived from the alignment of water and lipid headgroup dipoles.[43] Fig. 4 and S3† show the differential excitation spectra of di-8-ANEPPS in HBMEC, normal breast cells and cancer breast cells, at three different concentrations of PvD_1, as well as R_{norm}. $PvD1$ interacts with HBMEC in a way that perturbs membrane potential, i.e. inserting into the lipid bilayer. Interaction with breast cells is more superficial as the dye does not report the presence of the defensin. The accumulation of this peptide in the membrane is not sufficient to induce severe damage to the cell membrane. Similar to HBMEC, MCF 10A and MDA-MB-231 cells are capable of attracting PvD_1 to their surface. The higher negative membrane surface charge compared with HBMEC allows a significant change in zeta potential values for the breast cells. The partial accumulation of the peptide in the surface of the lipid bilayer of non-tumor breast cells results in transient changes of the membranes' dipole potential which are not reported by the hydrophobic dye.

Cell-to-cell adhesion as a potential control point to target brain metastasis. Correlation with PvD_1–cellular membrane interaction

Metastatic breast cancer cells transmigrate through the layer of endothelial cells of brain capillaries before settling in the brain.[31] In addition to protecting the brain, the BBB also protects metastatic cells in the processes of extravasation and multiplication[11,31] by actively helping cancer cells to reach the brain parenchyma and providing an optimum medium for further proliferation.[11] The cellular and molecular mecha-

nisms underlying the interaction of metastatic cells with brain endothelial cells are important during these events but remain largely unknown. The characterization of this interaction should however occur at the early steps of cell–cell interaction since metastatic brain tropism relies on the first contact.[44] Adhesion plays important roles in cell communication and regulation of signalling pathways in cancer[45–47] and its changes result in perturbations on biophysical and biochemical cellular processes necessary to maintain cell homeostasis. Many techniques have been used to measure cell adhesion and these can be applied to a cell population or in a single cell approach.[47–49] Allowing the measurement of forces in the pN to nN range with a displacement of sub-nm to μm under near physiological conditions,[30,50] AFM represents an ideal method for characterizing cell-to-cell interactions.[46]

We tested PvD_1 ability to interfere with cell-to-cell adhesion in breast cancer cells and attachment of cancer cells to brain endothelial cells using AFM-SCFS (Fig. 5, S4 and S5†). A single living cell was captured with a biotin BSA-ConA-streptavidin coated tipless cantilever which converted the cell into a probe for making contact with other cells. MDA-MB-231 tumor cells were attached to cantilevers as described previously and approached to MDA-MB-231 and PvD_1-treated cells. The contact was maintained for 5 seconds with a constant force of 0.5 nN. Cell detachment was recorded during retraction of the
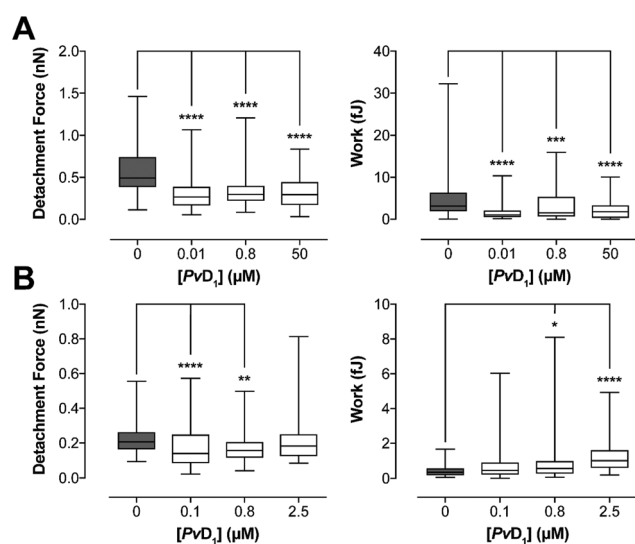

Fig. 5 Cell-to-cell adhesion investigated by atomic force microscopy-based-single cell force spectroscopy (AFM-SCFS). PvD_1 perturbs cell-to-cell adhesion between breast tumor cells and endothelial cells. Adhesion strength (F_D, left graph) and work (W_D, right graph) in the absence and presence of peptide are presented for MDA-MB-231 cells – MDA-MB-231-cantilever bound cells (A) and HBMEC – MDA-MB-231-cantilever bound cells (B). 16 to 28 cells were analyzed and the number of force–distance curves obtained for each peptide concentration tested was: (A) 0 μM – 65; 0.01 μM – 63; 0.8 μM – 47 and 50 μM – 54; (B) 0 μM – 97; 0.1 μM – 123; 0.8 μM – 63 and 2.5 μM – 59. Statistical significance was evaluated with a Kruskal–Wallis test. *0.01 < p-value < 0.05; **0.001 < p-value < 0.01; ***0.0001 < p-value < 0.001; ****p-value < 0.0001.

cantilever (force–distance, F–d curves, Fig. S4†); adhesion was characterized by the determination of the maximum detachment force (F_D) and the work of detachment (W_D). F_D corresponds to the peak of adhesion force with respect to the zero-force level[47] and relates to the force necessary to detach both cells. W_D is used to describe the energy needed for detaching the cell probe and corresponds to the integrated area of detachment below the zero-force level and the contour of the F–d curve.[47] W_D results from adhesive elements from the rupture of formed complexes and the mechanical component resulting from cell deformation. After the maximum detachment force occurs it is typical to find step-like events which correspond to the unbinding or destruction of adhesive units.[47] During the detachment process surface membrane nanotubes (tethers) can be extracted from the membrane. This occurs when the lipid bilayer is pulled away from the cortical cytoskeleton forming thin-like protrusions.[47] In these cases, in which tethers are formed, the F–d curve is characterized by forces that culminate with the detachment of the nanotube from the cell.[51] We have analysed tether formation after the initial part of the F–d retraction curves (>3 μm); in the initial part of the F–d curve other type of unbinding events are dominant.[30]

Tumor–tumor cell adhesion results are presented in Fig. 5A and S5.† F_D, W_D and tether extraction force decrease in the presence of the PvD_1 peptide. PvD_1 ability in reducing the adhesiveness of tumor cells might contribute for preventing or retarding the formation of a solid tumor mass in the breast. Damage to the tumor cells induces changes in the cell cytoskeleton which contribute to perturbation in adhesion, to a lower energy necessary to detach tumor cells from each other and to changes in the tether extraction forces. The observation of
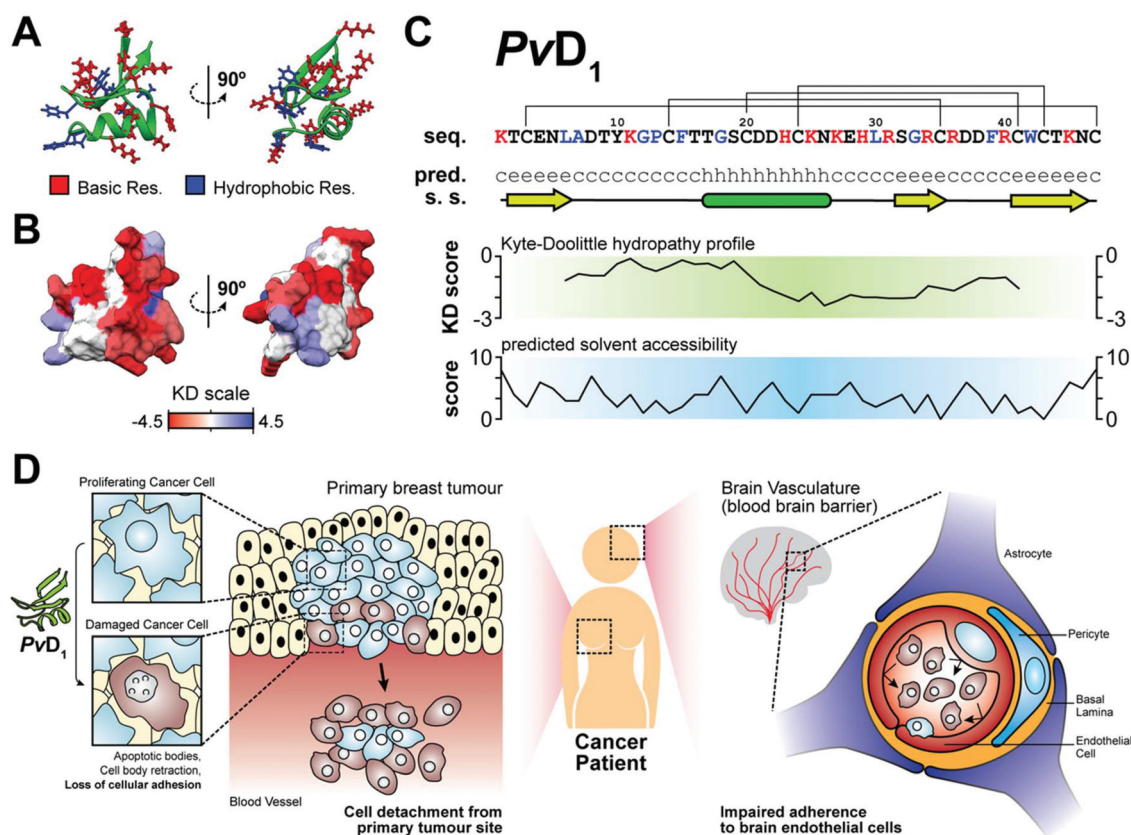
Fig. 6 The natural PvD_1 defensin as an alternative therapeutic for metastatic breast cancer. (A, B, C) PvD_1 structural features evidenced by homology and sequence based predictions. Homology based simulation of PvD_1 tri-dimensional structure was obtained using the I-Tasser online server.[56–58] PDB entry 2GL1, corresponding to the VrD2 defensin, was selected as a structural homology template. Tri-dimensional representations highlighting the secondary structure motifs and basic/hydrophobic amino acid residue localization (A), and the Kyte−Doolittle hydropathy surface profile (B) are shown from two orthogonal perspectives. The PvD_1 amino acid residue sequence, secondary structure tendency per residue, Kyte−Doolittle hydropathy plot (obtained using ExPaSy ProtScale with an 11 amino acid window)[59] and solvent accessibility scores are also shown (C). Lines represented above the PvD_1 sequence correspond to the predicted disulphide bonds between cysteine residues. Basic and hydrophobic amino acid residues are highlighted within the PvD_1 sequence in red and blue, respectively. Random coils (c), β-sheets (e) and α-helices (h) are depicted as a full line, an arrow and a rounded box, respectively. (D) The PvD_1 putative mode of action in an *in vivo* context. PvD_1 modulates the viability and cellular adhesion properties of proliferating breast cancer cells. Damaged cells detach from the primary tumor site and are carried through the blood stream to other organs. Circulating cancer cells become more susceptible to PvD_1 action. Upon reaching the brain vasculature, protected by the BBB, circulating damaged cells are unable to efficiently attach to the brain endothelial cell wall. $PvD1$ accumulates in endothelial cell membranes, which may act as a latent reservoir. Consequently, cancer cell extravasation and metastasis are greatly impaired.

tethers depends on the adhesive and elastic properties of the cell[52] and changes in their associated extraction forces have been reported to translate alterations in membrane–cytoskeleton coupling.[30,51] These observations consequently point to an internal extensive cell damage caused by the PvD_1 peptide that challenges the tumor mass formation.

However, forming less adhesive breast cancer cells can facilitate their entrance into blood circulation and, consequently, spreading of metastasis formation stimulation. We thus decided to investigate the changes occurring in F_D and W_D after promoting contact between a HBMEC captured cell and breast tumor cells (Fig. S3†). Low PvD_1 concentrations, not enough to induce low levels of cell death, are sufficient to perturb the adhesion between tumor–brain endothelial cells. The observed decrease in F_D and W_D is accompanied by an increase in tether extraction force reflecting changes at the cytoskeleton level of the HBMEC bound to the cantilever (Fig. S5†). In this experimental setup, we were not able to obtain good signal-to-noise F–d curves when treating tumor cells with higher PvD_1 concentration before interaction with brain captured cells. The degree of tumor cell destruction did not allow proper contact with a single captured HBMEC. PvD_1 is therefore reducing cell-to-cell adhesion of both breast tumor cells among themselves and between tumor cells and brain endothelial cells. Metastatic adhesion to BBB cells is abrogated by PvD_1.

PvD_1-treated HBMEC interaction with a cantilever-bound breast tumor cell resulted in decreased F_D but higher W_D at the tether extraction force (Fig. 5 and S5†). These results reveal that cell detachment in this case is not an abrupt event and that intercellular connections are not disrupted simultaneously which affects the area under the curve resulting in more energy recruited in the process.[53] Differences in W_D account not only for adhesion but also for mechanical components of the cell which are difficult to completely isolate and in turn depend on the cell's viscoelastic properties.[52] Changes in the HBMEC's biomechanics after PvD_1 treatment will contribute to increasing difficulty in BBB crossing by breast tumor cells.

Conclusions

In this study we show the activity of a natural peptide on human breast and brain endothelial cells. PvD_1 is a highly cytotoxic peptide towards human breast cancer cells when compared to HNP-1. AFM (imaging and SCFS), zeta potential and fluorescence spectroscopy techniques reveal that PvD_1 interacts differently with the cell membrane of normal and tumor cells without inducing full membrane neutralization prior to the onset of toxicity. The peptide reaches the interior of the breast tumor cells inducing apoptotic events. In normal brain cells PvD_1 partially accumulates in the cellular membrane resulting in perturbations on the membrane's dipole potential whose magnitude is proposed to be affected by the different membrane features of these cells.

Our observations are supported by structural data obtained from PvD_1 peptide homology based prediction (Fig. 6).[54] PvD_1 concentrates part of its hydrophobic amino acid residues on one side of its surface. Albeit not being supercharged (predicted net charge +1.4), PvD_1 has a high density of cationic residues in a second separate region, thus being highly amphipathic, which is in agreement with its ability to internalize the cells and reach intracellular targets.

PvD_1 is also a modulator of cell-to-cell adhesion since it is not only promoting de-adhesion of tumor cells, reducing the F_D and W_D necessary for this event to occur, but it also perturbs tumor cell adhesion to endothelial brain cells.

This is the first report on the biophysical characterization of peptide–HBMEC interaction using zeta potential techniques and AFM in imaging and SCFS modes. Suppression of cancer cell adhesion is a promising strategy to debilitate cancer metastatic spreading[55] and our results indicate that PvD_1 can be explored as an alternative strategy to invasive approaches such as breaching the BBB by preventing metastatic cells from attaching to its surface.

Conflicts of interest

There are no conflicts to declare.

Author contributions

T. N. F., F. D. O., M. A. R. B. C. and D. G. designed the experiments. T. N. F., F. D. O., I. A., and D. G. performed the experimental work and data analysis. E. O. M. and V. M. G. performed the peptide synthesis. All authors contributed to data interpretation and discussion. T. N. F., M. A. R. B. C. and D. G. wrote the manuscript with contributions from all the authors. All authors approved the final version of the manuscript.

Acknowledgements

References

1 C. DeSantis, J. Ma, L. Bryan and A. Jemal, Breast cancer statistics, 2013, *CA-Cancer J. Clin.*, 2014, **64**(1), 52–62. Available from: http://doi.wiley.com/10.3322/caac.21203.

2 F. Kamangar, G. M. Dores and W. F. Anderson, Patterns of Cancer Incidence, Mortality, and Prevalence Across Five Continents: Defining Priorities to Reduce Cancer Disparities in Different Geographic Regions of the World, *J. Clin. Oncol.*, 2006, **24**(14), 2137–2150. Available from: http://ascopubs.org/doi/10.1200/JCO.2005.05.2308.

3 S. Darby, P. McGale, C. Correa, C. Taylor, R. Arriagada, M. Clarke, *et al.*, Effect of radiotherapy after breast-conserving surgery on 10-year recurrence and 15-year breast cancer death: meta-analysis of individual patient data for 10 801 women in 17 randomised trials, *Lancet*, 2011, **378**(9804), 1707–1716, DOI: 10.1016/S0140-6736(11)61629-2.

4 C. Núñez, J. L. Capelo, G. Igrejas, A. Alfonso, L. M. Botana and C. Lodeiro, An overview of the effective combination therapies for the treatment of breast cancer, *Biomaterials*, 2016, **97**, 34–50.

5 R. A. Morshed, M. E. Muroski, Q. Dai, M. L. Wegscheid, B. Auffinger, D. Yu, *et al.*, Cell-Penetrating Peptide-Modified Gold Nanoparticles for the Delivery of Doxorubicin to Brain Metastatic Breast Cancer, *Mol. Pharm.*, 2016, **13**(6), 1843–1854. Available from: http://pubs.acs.org/doi/abs/10.1021/acs.molpharmaceut.6b00004.

6 B. C. Pestalozzi, D. Zahrieh, K. N. Price, S. B. Holmberg, J. Lindtner, J. Collins, *et al.*, Identifying breast cancer patients at risk for Central Nervous System (CNS) metastases in trials of the International Breast Cancer Study Group (IBCSG), *Ann. Oncol.*, 2006, **17**(6), 935–944. Available from: https://academic.oup.com/annonc/article-lookup/doi/10.1093/annonc/mdl064.

7 X. Cheng and M.-C. Hung, Breast cancer brain metastases, *Cancer Metastasis Rev.*, 2007, **26**(3–4), 635–643. Available from: http://www.ncbi.nlm.nih.gov/pubmed/17717635.

8 S. Saadatmand, E. M. de Kruijf, A. Sajet, N. G. Dekker-Ensink, J. G. H. van Nes, H. Putter, *et al.*, Expression of cell adhesion molecules and prognosis in breast cancer, *Br. J. Surg.*, 2013, **100**(2), 252–260. Available from: http://doi.wiley.com/10.1002/bjs.8980.

9 N. U. Lin, J. R. Bellon and E. P. Winer, CNS Metastases in Breast Cancer, *J. Clin. Oncol.*, 2004, **22**(17), 3608–3617. Available from: http://ascopubs.org/doi/10.1200/JCO.2004.01.175.

10 Y. Tsukada, A. Fouad, J. W. Pickren and W. W. Lane, Central nervous system metastasis from breast carcinoma, Autopsy study, *Cancer*, 1983, **52**(12), 2349–2354. Available from: http://doi.wiley.com/10.1002/1097-0142%2819831215%2952%3A12%3C2349%3A%3AAID-CNCR2820521231%3E3.0.CO%3B2-B%5Cn(null).

11 N. U. Lin, L. Amiri-Kordestani, D. Palmieri, D. J. Liewehr and P. S. Steeg, CNS Metastases in Breast Cancer: Old Challenge, New Frontiers, *Clin. Cancer Res.*, 2013, **19**(23), 6404–6418. Available from: http://clincancerres.aacrjournals.org/cgi/doi/10.1158/1078-0432.CCR-13-0790.

12 P. R. Lockman, R. K. Mittapalli, K. S. Taskar, V. Rudraraju, B. Gril, K. A. Bohn, *et al.*, Heterogeneous Blood-Tumor Barrier Permeability Determines Drug Efficacy in Experimental Brain Metastases of Breast Cancer, *Clin. Cancer Res.*, 2010, **16**(23), 5664–5678. Available from: http://clincancerres.aacrjournals.org/cgi/doi/10.1158/1078-0432.CCR-10-1564.

13 S. Motl, Y. Zhuang, C. M. Waters and C. F. Stewart, Pharmacokinetic Considerations in the Treatment of CNS Tumours, *Clin. Pharmacokinet.*, 2006, **45**(9), 871–903. Available from: http://link.springer.com/10.2165/00003088-200645090-00002.

14 S. Ohtsuki and T. Terasaki, Contribution of Carrier-Mediated Transport Systems to the Blood–Brain Barrier as a Supporting and Protecting Interface for the Brain; Importance for CNS Drug Discovery and Development, *Pharm. Res.*, 2007, **24**(9), 1745–1758. Available from: http://link.springer.com/10.1007/s11095-007-9374-5.

15 R. Sun, L.-Y. Zhang, L.-S. Chen and Y. Tian, Long-term outcome of changes in cognitive function of young rats after various/different doses of whole brain irradiation, *Neurol. Res.*, 2016, **38**(7), 647–654. Available from: http://www.tandfonline.com/doi/full/10.1080/01616412.2016.1188483.

16 I. Tonning Olsson, S. Perrin, J. Lundgren, L. Hjorth and A. Johanson, Long-Term Cognitive Sequelae After Pediatric Brain Tumor Related to Medical Risk Factors, Age, and Sex, *Pediatr. Neurol.*, 2014, **51**(4), 515–521, DOI: 10.1016/j.pediatrneurol.2014.06.011.

17 A. F. Eichler, E. Chung, D. P. Kodack, J. S. Loeffler, D. Fukumura and R. K. Jain, The biology of brain metastases—translation to new therapies, *Nat. Rev. Clin Oncol.*, 2011, **8**(6), 344–356. Available from: http://www.pubmed central.nih.gov/articlerender.fcgi?artid=3259742&tool=pmcentrez&rendertype=abstract.

18 D. Gaspar, A. S. Veiga and M. A. R. B. Castanho, From antimicrobial to anticancer peptides. A review, *Front. Microbiol.*, 2013, **4**(Oct), 1–16. Available from: http://journal.frontiersin.org/article/10.3389/fmicb.2013.00294/abstract.

19 D. W. Hoskin and A. Ramamoorthy, Studies on anticancer activities of antimicrobial peptides, *Biochim. Biophys. Acta, Biomembr*, 2008, **1778**(2), 357–375.

20 E. J. Paredes-Gamero, R. L. Casaes-Rodrigues, G. E. D. D. Moura, T. M. Domingues, M. V. Buri, V. H. C. Ferreira, *et al.*, Cell-Permeable Gomesin Peptide Promotes Cell Death by Intracellular Ca2+ Overload, *Mol. Pharm.*, 2012, **9**(9), 2686–2697. Available from: http://pubs.acs.org/doi/abs/10.1021/mp300251j.

21 R. A. de Azevedo, C. R. Figueiredo, A. K. Ferreira, A. L. Matsuo, M. H. Massaoka, N. Girola, *et al.*, Mastoparan induces apoptosis in B16F10-Nex2 melanoma cells via the intrinsic mitochondrial pathway and displays antitumor activity in vivo, *Peptides*, 2015, **68**, 113–119, DOI: 10.1016/j.peptides.2014.09.024.

22 R. Gaglione, L. Pirone, B. Farina, S. Fusco, G. Smaldone, M. Aulitto, *et al.*, Insights into the anticancer properties of

the first antimicrobial peptide from Archaea, *Biochim. Biophys. Acta, Gen. Subj.*, 2017, **1861**(9), 2155–2164, DOI: 10.1016/j.bbagen.2017.06.009.

23 D. Gaspar, J. M. Freire, T. R. Pacheco, J. T. Barata and M. A. R. B. Castanho, Apoptotic human neutrophil peptide-1 anti-tumor activity revealed by cellular biomechanics, *Biochim. Biophys. Acta, Mol. Cell Res.*, 2015, **1853**(2), 308–316, DOI: 10.1016/j.bbamcr.2014.11.006.

24 P. D. Games, I. S. dos Santos, M. Éo, M. S. S. Diz, A. O. Carvalho, G. A. de Souza-Filho, *et al.*, Isolation, characterization and cloning of a cDNA encoding a new antifungal defensin from Phaseolus vulgaris L. seeds, *Peptides*, 2008, **29**(12), 2090–2100. Available from: http://linkinghub.elsevier.com/retrieve/pii/S0196978108003586.

25 E. O. Mello, S. F. F. Ribeiro, A. O. Carvalho, I. S. Santos, M. Da Cunha, C. Santa-Catarina, *et al.*, Antifungal Activity of PvD1 Defensin Involves Plasma Membrane Permeabilization, Inhibition of Medium Acidification, and Induction of ROS in Fungi Cells, *Curr. Microbiol.*, 2011, **62**(4), 1209–1217. Available from: http://link.springer.com/10.1007/s00284-010-9847-3.

26 C. Sinthuvanich, A. S. Veiga, K. Gupta, D. Gaspar, R. Blumenthal and J. P. Schneider, Anticancer β-Hairpin Peptides: Membrane-Induced Folding Triggers Activity, *J. Am. Chem. Soc.*, 2012, **134**(14), 6210–6217. Available from: http://pubs.acs.org/doi/abs/10.1021/ja210569f.

27 D. Nečas and P. Klapetek, Gwyddion: an open-source software for SPM data analysis, *Cent. Eur. J. Phys.*, 2012, **10**(1), 181–188. Available from: http://www.degruyter.com/view/j/phys.2012.10.issue-1/s11534-011-0096-2/s11534-011-0096-2.xml.

28 R. J. Clarke and D. J. Kane, Optical detection of membrane dipole potential: avoidance of fluidity and dye-induced effects, *Biochim. Biophys. Acta, Biomembr.*, 1997, **1323**(2), 223–239. Available from: http://linkinghub.elsevier.com/retrieve/pii/S0005273696001885.

29 P. M. Matos, M. A. R. B. Castanho and N. C. Santos, HIV-1 Fusion Inhibitor Peptides Enfuvirtide and T-1249 Interact with Erythrocyte and Lymphocyte Membranes, *PLoS One*, 2010, **5**(3), e9830, Available from: http://dx.plos.org/10.1371/journal.pone.0009830.

30 J. Friedrichs, J. Helenius and D. J. Muller, Quantifying cellular adhesion to extracellular matrix components by single-cell force spectroscopy, *Nat. Protoc.*, 2010, **5**(7), 1353–1361, DOI: 10.1038/nprot.2010.89%0AAtomic. Available from.

31 I. Wilhelm, J. Molnár, C. Fazakas, J. Haskó and I. Krizbai, Role of the Blood-Brain Barrier in the Formation of Brain Metastases, *Int. J. Mol. Sci.*, 2013, **14**(1), 1383–1411. Available from: http://www.mdpi.com/1422-0067/14/1/1383/.

32 D. Gaspar, A. S. Veiga, C. Sinthuvanich, J. P. Schneider and M. A. R. B. Castanho, Anticancer Peptide SVS-1: Efficacy Precedes Membrane Neutralization, *Biochemistry*, 2012, **51**(32), 6263–6265. Available from: http://pubs.acs.org/doi/abs/10.1021/bi300836r.

33 E. Canetta, A. Riches, E. Borger, S. Herrington, K. Dholakia and A. K. Adya, Discrimination of bladder cancer cells from normal urothelial cells with high specificity and sensitivity: Combined application of atomic force microscopy and modulated Raman spectroscopy, *Acta Biomater.*, 2014, **10**(5), 2043–2055. Available from: http://linkinghub.elsevier.com/retrieve/pii/S1742706113006624 [cited 2016 Sep 25].

34 P. Eaton, V. Zuzarte-Luis, M. M. Mota, N. C. Santos and M. Prudêncio, Infection by Plasmodium changes shape and stiffness of hepatic cells, *Nanomedicine*, 2012, **8**(1), 17–19, DOI: 10.1016/j.nano.2011.10.004.

35 D. B. Agus, J. F. Alexander, W. Arap, S. Ashili, J. E. Aslan, R. H. Austin, *et al.*, A physical sciences network characterization of non-tumorigenic and metastatic cells, *Sci. Rep.*, 2013, **3**(1), 1449, Available from: http://www.nature.com/srep/2013/130422/srep01449/full/srep01449.html.

36 M. Girasole, G. Pompeo, A. Cricenti, G. Longo, G. Boumis, A. Bellelli, *et al.*, The how, when, and why of the aging signals appearing on the human erythrocyte membrane: an atomic force microscopy study of surface roughness, *Nanomedicine*, 2010, **6**(6), 760–768, DOI: 10.1016/j.nano.2010.06.004.

37 S. Elmore, Apoptosis: A Review of Programmed Cell Death, *Toxicol. Pathol.*, 2007, **35**(4), 495–516. Available from: http://tpx.sagepub.com/content/35/4/495.full.

38 M. M. B. Ribeiro, M. M. Domingues, J. M. Freire, N. C. Santos and M. a. R. Castanho, Translocating the blood-brain barrier using electrostatics, *Front. Cell. Neurosci.*, 2012, **6**(October), 1–7. Available from: http://www.pubmedcentral.nih.gov/articlerender.fcgi?artid=3468918&tool=pmcentrez&rendertype=abstract.

39 M. J. Bernas, F. L. Cardoso, S. K. Daley, M. E. Weinand, A. R. Campos, A. J. G. Ferreira, *et al.*, Establishment of primary cultures of human brain microvascular endothelial cells to provide an in vitro cellular model of the blood-brain barrier, *Nat. Protoc.*, 2010, **5**(7), 1265–1272, DOI: 10.1038/nprot.2010.76.

40 G. M. Cooper and R. E. Hausman, *The cell. A molecular Approach*, Sinauer Associates, Inc., USA, 5th edn, 2009, pp. 530–532.

41 I. Dobrzynska, B. Szachowicz-Petelska, S. Sulkowski and Z. Figaszewski, Changes in electric charge and phospholipids composition in human colorectal cancer cells, *Mol. Cell. Biochem.*, 2005, **276**(1–2), 113–119.

42 H. S. Lee, C. B. Park, J. M. Kim, S. A. Jang, I. Y. Park, M. S. Kim, *et al.*, Mechanism of anticancer activity of buforin IIb, a histone H2A-derived peptide, *Cancer Lett.*, 2008, **271**(1), 47–55.

43 T. N. Figueira, A. S. Veiga and M. A. R. B. Castanho, The interaction of antibodies with lipid membranes unraveled by fluorescence methodologies, *J. Mol. Struct.*, 2014, **1077**, 114–120, DOI: 10.1016/j.molstruc.2014.02.037.

44 A. Drolez, E. Vandenhaute, S. Julien, F. Gosselet, J. Burchell, R. Cecchelli, *et al.*, Selection of a Relevant In Vitro Blood-Brain Barrier Model to Investigate Pro-Metastatic Features of Human Breast Cancer Cell Lines, *PLoS One*, 2016, **11**(3), e0151155, Available from: http://dx.plos.org/10.1371/journal.pone.0151155.

45 T. Okegawa, R.-C. Pong, Y. Li and J.-T. Hsieh, The role of cell adhesion molecule in cancer progression and its application in cancer therapy, *Acta Biochim. Pol.*, 2004, **51**(2), 445–457.

46 S. Park, J. Kim and S.-H. Yoon, A Review on Quantitative Measurement of Cell Adhesion Strength, *J. Nanosci. Nanotechnol.*, 2016, **16**(5), 4256–4273. Available from: http://openurl.ingenta.com/content/xref?genre=article&issn=1533-4880&volume=16&issue=5&spage=4256.

47 J. Friedrichs, K. R. Legate, R. Schubert, M. Bharadwaj, C. Werner, D. J. Müller, *et al.*, A practical guide to quantify cell adhesion using single-cell force spectroscopy, *Methods*, 2013, **60**(2), 169–178, DOI: 10.1016/j.ymeth.2013.01.006.

48 R. I. Litvinov, H. Shuman, J. S. Bennett and J. W. Weisel, Binding strength and activation state of single fibrinogen-integrin pairs on living cells, *Proc. Natl. Acad. Sci. U. S. A.*, 2002, **99**(11), 7426–7431. Available from: http://www.pnas.org/cgi/doi/10.1073/pnas.112194999.

49 M. Benoit, D. Gabriel, G. Gerisch and H. E. Gaub, Discrete interactions in cell adhesion measured by single-molecule force spectroscopy, *Nat. Cell Biol.*, 2000, **2**(6), 313–317. Available from: http://www.ncbi.nlm.nih.gov/pubmed/10854320%5Cnhttp://www.nature.com/doifinder/10.1038/35014000.

50 J. Helenius, C.-P. Heisenberg, H. E. Gaub and D. J. Muller, Single-cell force spectroscopy, *J. Cell Sci.*, 2008, **121**(11), 1785–1791. Available from: http://jcs.biologists.org/cgi/doi/10.1242/jcs.030999.

51 M. Tulla, J. Helenius, J. Jokinen, A. Taubenberger, D. J. Müller and J. Heino, TPA primes α2β1 integrins for cell adhesion, *FEBS Lett.*, 2008, **582**(23–24), 3520–3524, DOI: 10.1016/j.febslet.2008.09.022.

52 P.-H. Puech, A. Taubenberger, F. Ulrich, M. Krieg, D. J. Muller and C.-P. Heisenberg, Measuring cell adhesion forces of primary gastrulating cells from zebrafish using atomic force microscopy, *J. Cell Sci.*, 2005, **118**(18), 4199–4206. Available from: http://jcs.biologists.org/cgi/doi/10.1242/jcs.02547.

53 A. S. Ribeiro, F. A. Carvalho, J. Figueiredo, R. Carvalho, T. Mestre, J. Monteiro, *et al.*, Atomic force microscopy and graph analysis to study the P-cadherin/SFK mechanotransduction signalling in breast cancer cells, *Nanoscale*, 2016, **8**(46), 19390–19401. Available from: http://xlink.rsc.org/?DOI=C6NR04465D.

54 M. Éo, I. S. dos Santos, A. de O Carvalho, L. S. de Souza, G. A. de Souza-Filho, V. V. do Nascimento, *et al.*, Functional expression and activity of the recombinant antifungal defensin PvD1r from Phaseolus vulgaris L. (common bean) seeds, *BMC Biochem.*, 2014, **15**(1), 7, Available from: http://www.biomedcentral.com/1471-2091/15/7.

55 R. Schmidmaier and P. Baumann, ANTI-ADHESION Evolves To a Promising Therapeutic Concept in Oncology, *Curr. Med. Chem.*, 2008, **15**(10), 978–990. Available from: http://www.eurekaselect.com/openurl/content.php?genre=article&issn=0929-8673&volume=15&issue=10&spage=978.

56 Y. Zhang, I-TASSER server for protein 3D structure prediction, *BMC Bioinf.*, 2008, **9**(1), 40. Available from: http://www.ncbi.nlm.nih.gov/pubmed/18215316%5Cn, http://www.pubmedcentral.nih.gov/articlerender.fcgi?artid=PMC2245901.

57 A. Roy, A. Kucukural and Y. Zhang, I-TASSER: a unified platform for automated protein structure and function prediction, *Nat. Protoc.*, 2010, **5**(4), 725–738. Available from: http://www.nature.com/doifinder/10.1038/nprot.2010.5.

58 J. Yang, R. Yan, A. Roy, D. Xu, J. Poisson and Y. Zhang, The I-TASSER Suite: protein structure and function prediction, *Nat. Methods*, 2014, **12**(1), 7–8, DOI: 10.1038/nmeth.3213.

59 E. Gasteiger, C. Hoogland, A. Gattiker, S. Duvaud, M. R. Wilkins, R. D. Appel, *et al.* Protein Identification and Analysis Tools on the ExPASy Server, in *The Proteomics Protocols Handbook*, Humana Press, Totowa, NJ, 2005, pp. 571–607. Available from: http://link.springer.com/10.1385/1-59259-890-0:571.